ISSN 2706-655X Vol.6, Issue 1: 120-124, DOI: 10.25236/IJFET.2024.060119

Optoelectronic synapses based on MZO/AZO heterojunction

Zhaoyuan Fan[1,a], Zhenghua Tang[1,b,*]

[1]*School of Physics and Optoelectric Engineering, Guangdong University of Technology, Guangzhou Higher Education Mega Center, Guangzhou, 510006, China*
[a]*2112115054@mail2.gdut.edu.cn*, [b]*tangzh@gdut.edu.cn*
[*]*Corresponding author*

Abstract: *In contrast to purely electronic neuromorphic devices, neuromorphic devices stimulated by light Neuromorphic devices stimulated by optical signals are gaining attention for their realistic sensory simulation. A transparent optoelectronic neuromorphic device based on a Mg-doped ZnO/Al-doped ZnO (MZO/AZO) heterostructure memristor has been fabricated in this study. It responds to both electrical and optical signals and successfully simulates various synaptic behaviours, such as STP, LTP, and PPF. In addition, the photomemory mechanism was identified by analysing the energy band structures of MZO and AZO.*

Keywords: *MZO/AZO, Optoelectronic, Artificial synapse*

1. Introduction

The rapid expansion of data and information due to bottlenecks in the von Neumann architecture is placing increasing demands on the efficiency of computer capture and processing [1-3]. In the human brain, 10^{11} nerve cells are connected by 10^{14} synapses to form a neural network that can effectively process huge amounts of data. To overcome von Neumann's bottleneck, artificial synapses based on electronic devices such as memristors and field-effect transistors have been studied to imitate the basic computational functions of the nervous system by modulating the conductance (synaptic weight) of the devices, called "synaptic plasticity". Based on the properties of synapses and neurons, researchers have come up with a number of novel devices to implement artificial synapses, such as memristor [4], phase change memory(PCM), magnetic random access memory(MRAM) [5] and ferroelectric field-effect transistors(FeFET) [6]. Each devices has its own advantages and disadvantages, such as PCM and MRAM, which have developed over a long period of time and now have the ability to mass produce, but their conductance is usually under the action of the pulse to produce a sudden change in the analog characteristics that need to be improved; FeFET have excellent analog characteristics, but the three-terminal configuration is not conducive to integration.

In contrast, there may be better prospects for implementing artificial synapses through memristors, which are circuit devices with a memory effect, usually a metal/insulator/metal sandwich structure where the metal serves as the upper and lower electrodes and the insulating layer serves as the resistive layer. The modulation of the conductance value of the device can be achieved in the presence of an applied electric field. Currently, researchers have achieved the preparation of memristors based on a variety of materials, such as oxides [7], organics [8], and perovskites [9], among which metal oxide-based amnesia has the highest compatibility with existing CMOS device fabrication processes and is most likely to be realized in the short term. Neurons generate postsynaptic currents (PSC) in response to external stimuli, which are used for signal delivery and storage. The synaptic weight, also known as the value of the PSC, reflects the strength of the connection between two neurons. Changes in synaptic weight can be categorised into short-term plasticity (STP) and long-term plasticity (LTP) based on duration [10]. Further research has explored multiple plasticities of artificial synaptic devices, including paired-pulse facilitation (PPF) [11] and spike-timing-dependent plasticity (STDP) [12].

Neuromorphic devices for photonic stimulation offer a non-contact writing method that may enhance processing speed compared to devices solely activated electrically. For example, Shrivastava et al. successfully fabricated a light stimulated synaptic memristor (LSSM) based on ZnO/Zn_2SnO_4 heterostructure with reversibly tunable conductance state properties [13]. The synaptic features of this memory synapse, which is totally regulated by light, were identified through the effects of violet and red

ISSN 2706-655X Vol.6, Issue 1: 120-124, DOI: 10.25236/IJFET.2024.060119

light pulses, which either enhanced or inhibited its activity. Yu et al. developed a new optoelectronic neuromorphic device using pn junction-modified oxide thin-film transistors [14]. This device can process a wide range of visual data from ultraviolet to visible light in the neuromorphic system.

In this work, based on a heterojunction (AZO/MZO) with a bilayer structure, an optoelectronic artificial synaptic Au/AZO/MZO/FTO device has been fabricated. The device exhibits favourable electrosynaptic properties and effectively replicates the behaviours of biological synapses, including PSC, STP, LTP. In addition, the device's flexibility is improved by violet light pulses that create holes, altering the device's conductivity by extracting electrons from interfacial oxygen vacancies (V_O^S). The number of light pulses used was raised to model the transition from short-term memory (STM) to long-term memory (LTM).

2. Experimental section

2.1. Devices Fabrication

Ultrasonically treated FTO was used as the transparent substrate, Au as the bottom electrode and the top electrode, AZO and MZO as the interlayer. The preparation of the device includes the following processing steps.

First, the substrate was ultrasonically cleaned with acetone for 10 min. Then the interlayer was prepared on FTO by radio-frequency (RF) magnetron sputtering and deposited at room temperature for 40 mins. Adopting AZO (AZO: ZnO to Al_2O_3=98:2 wt%) target prepares AZO thin film and MZO target prepares MZO thin film. The experimental parameters were as follows: pressure 0.5 Pa, Ar gas flow rate 55 sccm, RF power 60 W, and sputtering time 40 mins. The top electrodes were plated on the sample using a small high-vacuum coating machine with a diameter of 1 mm and a mask template with a diameter of 1 mm at room temperature for the 120s to form a top-bottom (TB) electrode structure.

2.2. Device characterization

The UV–vis spectrophotometer (UV-3600 Plus) was used to record transmittance spectra. In addition, a Keithley 2611 semiconductor analyzer was used to measure and study the artificial synaptic behavior of the device.

3. Results and discussion

The device exhibits significant transmittance (>60%) in the visible light spectrum ranging from 400 nm to 800 nm, as shown in Fig. 1(a). Fig. 1(b) displays the optical photograph of the original device.

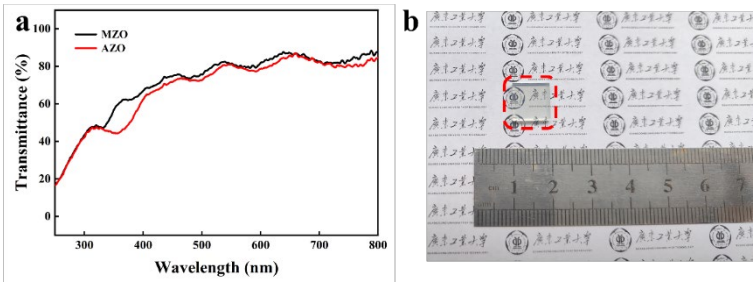

Figure 1: (a) Transmittance spectrum over the visible range; (b) optical photograph of the original device.

Fig. 2(a) shows the similarity between a biological synapse and a memristor: a channel represented by the PSC(postsynaptic currents) imitates the electrical impulse signal of the top electrode triggered by a presynaptic neuron. The channel aligns with a conductance comparable to the synaptic weight. Fig. 2(b) shows the I-V curve of the device during a voltage sweep ranging from -1 V to 1 V. The device exhibits a significant rectification ratio, similar to to a diode, because of the interaction between the ZnO and the FTO. The memristor has a significant nonlinearity in the forward direction, which helps regulate its conductance. The device's conductance increases or decreases constantly with positive or negative voltage sweeps, as shown in Fig. 2(c) and (d). Additionally, the conductance increment diminishes with each successive sweep. When the device conductance is considered a synaptic weight, it can be

ISSN 2706-655X Vol.6, Issue 1: 120-124, DOI: 10.25236/IJFET.2024.060119

considered a synaptic enhancement (inhibition) process. Furthermore, the device's enhancement and inhibition features are reproducible. Transitioning from short-term potentiation/short-term depression to long-term potentiation/long-term depression can be accomplished by delivering recurrent spikes to the device. LTP and LTD are the primary synaptic functions involved in the learning process, which are replicated by gradually modifying the conductance state of the Au/AZO/MZO/FTO device. As shown in Fig. 2(e) and (f), in order to achieve the transition from STP to LTP, we applied 100 pulses to our device with a voltage magnitude of ±1.0 V. The current of the device was gradually increased or decreased by the pulse stimulation.

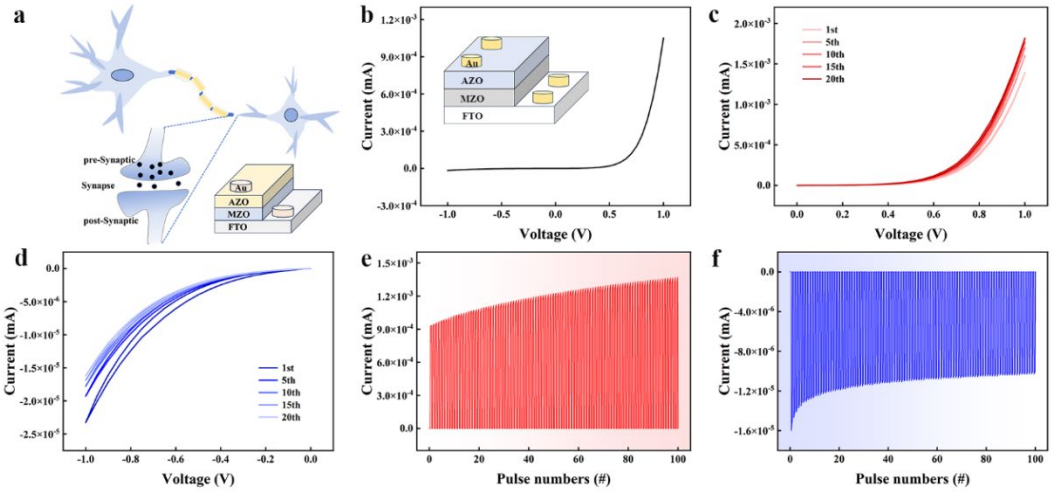

Figure 2: (a) Schematic diagram of synapse in the biological system and memristor device used as an artificial synapse. (b) Single I-V measurement curve of Au/AZO/MZO/FTO memristor (1.0 V to -1.0 V). (c) I-V curve under the forward voltage bias sweep (0 to 1.0 V). (d) IeV curve under reverse voltage bias sweep (0 to -1.0 V). The LTP and LTD effects of the devices are shown in (e) and (f).

Electrical activity and inputs from the external environment, particularly light signals, have an impact on synaptic plasticity in the nervous system. Different levels of light can cause changes in action potentials that are generated at synapses. These changes can be controlled dynamically, which changes the weights of synapses through neuronal activity. Such light-stimulus-dependent changes can be considered as light-induced plasticity. As shown in Fig. 3(a), the current response to the second light stimulus is significantly larger than that to the first light stimulus. It can also be noted that the current after the response is higher than the initial current before the stimulation and can last for a short time. Therefore, the PSCs after the first and second peaks are denoted as I_1 and I_2, respectively. and the PPF index is defined by the following equation:

$$PPF = \frac{I_2 - I_1}{I_1} \times 100\%$$

Fig. 3(b) shows the empirically determined PPF index and PPF index curve.The relationship between the PPF index and Δt can be modelled using the double exponential formula as follows:

$$PPF = C_1 e^{-\frac{t}{\tau_1}} + C_2 e^{-\frac{t}{\tau_2}}$$

C_1 and C_2 are the initial facilitation of each phase, and the relaxation time constants τ_1 and τ_2 are the fast and slow decay terms of the function, respectively. For the PPF feature, τ_1 and τ_2 were fitted to 104.82 ms and 138.54 ms, respectively, which is consistent with the relaxation factors in biological synapses.

Memory is divided into short-term and long-term memory, the difference being an increase in the relaxation time constant after stimulation, and the conversion of short-term memory (STM) into long-term memory (LTM) through repeated stimulation and reinforcement. We replicated the synaptic transition from STM to LTM by increasing the width and number of light pulses used by the device in the dark. As shown in Fig. 3(c), the PSC increased from 2.513 μA to 3.749 μA under photostimulation pulses with widths of 250 ms, 500 ms, and 750 ms. As shown in Fig. 3(d), the PSC increased from 1.025 μA to 3.133 μA under photostimulation pulses with quantities of 1, 10, 20, and 30. In addition, it can also be observed that the end of the pulse After 30 pulse responses, the rate of current decay decreased. The memory retention curves during the forgetting process as a function of time after the nth rehearsal, which are fitted well by using the Kohlrausch stretched exponential function:

ISSN 2706-655X Vol.6, Issue 1: 120-124, DOI: 10.25236/IJFET.2024.060119

$$I(t) = I_0 \exp[-(\frac{t}{\tau})^{\beta}]$$

where I (t) is the momentary PSC and I0 is the maximum PSC after stimulation; τ is the relaxation time constant; and β is the stretch index from 0 to 1. In this case, the decay rate of I(t)/I0 decreases with the number of light pulses, a phenomenon that can be described as memory preservation during forgetting.

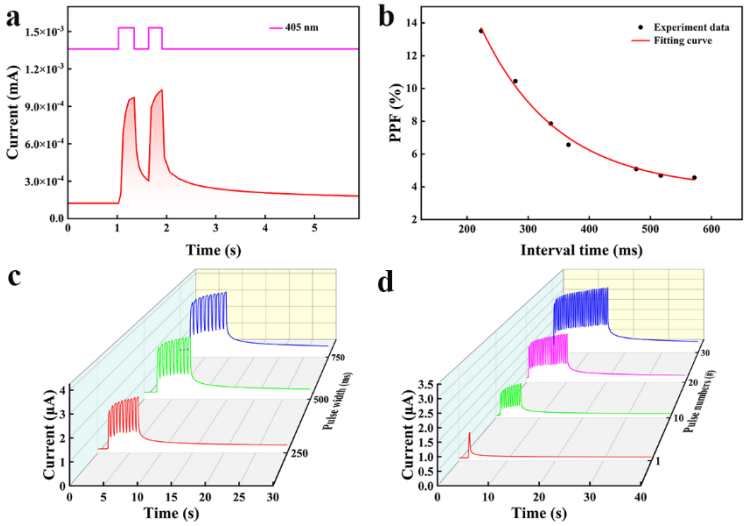

Figure 3: (a) Paired violet pulse triggers PSC on the artificial synapse. (b) The relationship between PPF and interval time (ΔT). (c) The PSC was excited with light pulses of a fixed wavelength of 405 nm and different widths. (d) The PSC was stimulated with a constant wavelength of 405 nm and an altering number of light pulses.

As shown in Fig. 4, the optical switching mechanism was established by examining the energy band structures of AZO and MZO. An electric field is created at the AZO/MZO interface because to the heterojunction. A possible well forms on the MZO side, whereas a potential barrier forms on the AZO side. The breadth of the interfacial potential barrier is determined by the concentration of charged V_O^S and is essential in influencing memory switching behavior. Typically, in n-type semiconductor oxides, defects such as V_O^S exhibit insulating α-type behavior in their neutral stable state (V_O^0) and β-type behavior in their substable charged state (V_O^{1+} or V_O^{2+}). In our work, the charged states of V_O^S can be achieved by trapping excited holes near the valence band maximum (VBM) at low bandgap excitations (hν < Eg). In theory, these kinds of hole-mediated leaps are possible because holes can be excited from defects in acceptors by taking in photons with energies less than the bandgap.

$$V_O^0 + O_{wb}^{2-} + 2h^+ \rightarrow \frac{V_O^{2+}}{O_i} + 2e^-$$

Here, O_{wb}^{2-} is weakly bound oxygen, and O_i is tissue oxygen. When the device is irradiated with purple irradiation (≈3.06 eV), then V_O^0 is photoionized into V_O^{2+}, leading to an increase in PSC.

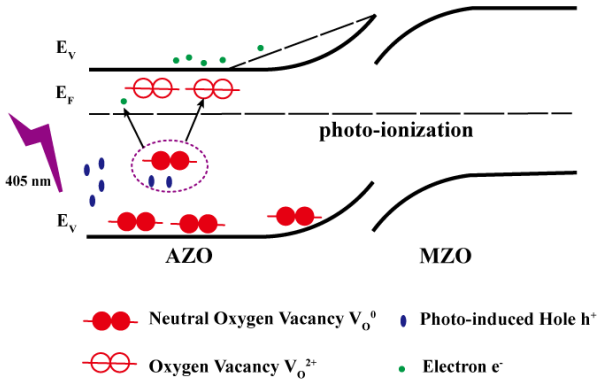

Figure 4: Photo-ionization and deionization of oxygen vacancies upon visible light stimulation

ISSN 2706-655X Vol.6, Issue 1: 120-124, DOI: 10.25236/IJFET.2024.060119

4. Conclusions

In summary, we have prepared a photovoltaic artificial synapse based on the AZO/MZO heterostructure, which has excellent electrosynaptic properties. The device has excellent electrosynaptic properties, and holes induced by a 405 nm UV light source can change the conductive state of the device by removing electrons from the interfacial oxygen vacancies (VOs), which causes the device to exhibit optical storage blocking behavior and successfully simulates the transition of biological synapses from STM to LTM.

Acknowledgements

This work was financially supported by the National Natural Science Foundation of China (NSFC) (Grant No. 51702055, 12172093, 62073084, 11904056, and 11704079).

References

[1] Song S; Choi C; Ahn J, et al. Artificial optoelectronic synapse based on spatiotemporal irradiation to source-sharing circuitry of synaptic phototransistors [J]. InfoMat, 2024, 6(2): e12479
[2] Sebastian A; Pannone A; Subbulakshmi R S, et al. Gaussian synapses for probabilistic neural networks [J]. Nature Communications, 2019, 10: 4199.
[3] Lee Y, Park H, Kim Y, et al. Organic electronic synapses with low energy consumption[J]. Joule, 2021, 5: 794-810.
[4] Islam R, Li H, Chen P-Y, et al. Device and materials requirements for neuromorphic computing[J]. Journal of Physics D: Applied Physics, 2019, 52(11): 113001.
[5] Tuma T, Pantazi A, Le Gallo M, et al. Stochastic phase-change neurons[J]. Nature Nanotechnology, 2016, 11(8): 693-699.
[6] Dutta S, Schafer C, Gomez J, et al. Supervised learning in all Fe FET-based spiking neural network: Opportunities and challenges[J]. Frontiers in Neuroscience, 2020, 14(1): 634.
[7] Lv D, Yang Q, Chen Q, et al. All-metal oxide synaptic transistor with modulatable plasticity[J]. Nanotechnology, 2020, 31(6): 65201.
[8] Kim S J, Lee T H, Yang J, et al. Vertically aligned two-dimensional halide perovskites for reliably operable artificial synapses[J]. Materials Today, 2022, 52: 19-30.
[9] Liu Q, Liu Y, Li J, et al. Fully Printed All-Solid-State Organic Flexible Artificial Synapse for Neuromorphic Computing [J]. ACS Applied Materials & Interfaces, 2019, 11(18): 16749-16757.
[10] Kim M, Lee J. Short-Term Plasticity and Long-Term Potentiation in Artificial Biosynapses with Diffusive Dynamics [J]. ACS Nano, 2018, 12(2): 1680-1687.
[11] Lee K C, Li M, Chang Y H, et al. Inverse paired-pulse facilitation in neuroplasticity based on interface-boosted charge trapping layered electronics[J]. Nano Energy, 2020, 77: 105258.
[12] Hao Y, Huang X, Dong M, et al. A biologically plausible supervised learning method for spiking neural networks using the symmetric STDP rule[J]. Neural Netwoks, 2020, 121: 387-395.
[13] Shrivastava S, Keong L B, Pratik S, at al. Fully Photon Controlled Synaptic Memristor for Neuro-Inspired Computing [J]. Advanced Electronic Materials, 2023, 9(3): 2201093.
[14] Yu J J, Liang L Y, Hu L X, et al. Optoelectronic neuromorphic thin-film transistors capable of selective attention and with ultra-low power dissipation[J]. Nano Energy, 2019, 62:772-780.